



3 4456 0145693 2

ORNL/TM-10200

# ornl

**OAK RIDGE  
NATIONAL  
LABORATORY**

**MARTIN MARIETTA**

## Effects of Isotropic Alpha Populations on Tokamak Ballooning Stability

D. A. Spong  
D. J. Sigmar  
K. T. Tsang

J. J. Ramos  
D. E. Hastings  
W. A. Cooper

OAK RIDGE NATIONAL LABORATORY

CENTRAL RESEARCH LIBRARY

CIRCULATION SECTION

4500N ROOM 175

**LIBRARY LOAN COPY**

DO NOT TRANSFER TO ANOTHER PERSON

If you wish someone else to see this  
report, send in name with report and  
the library will arrange a loan.

UCN-7969 (3 9-77)

OPERATED BY  
MARTIN MARIETTA ENERGY SYSTEMS, INC.  
FOR THE UNITED STATES  
DEPARTMENT OF ENERGY

Printed in the United States of America. Available from  
National Technical Information Service  
U.S. Department of Commerce  
5285 Port Royal Road, Springfield, Virginia 22161  
NTIS price codes—Printed Copy: A04; Microfiche A01

This report was prepared as an account of work sponsored by an agency of the United States Government. Neither the United States Government nor any agency thereof, nor any of their employees, makes any warranty, express or implied, or assumes any legal liability or responsibility for the accuracy, completeness, or usefulness of any information, apparatus, product, or process disclosed, or represents that its use would not *infringe* privately owned rights. Reference herein to any specific commercial product, process, or service by trade name, trademark, manufacturer, or otherwise, does not necessarily constitute or imply its endorsement, recommendation, or favoring by the United States Government or any agency thereof. The views and opinions of authors expressed herein do not necessarily state or reflect those of the United States Government or any agency thereof.

Fusion Energy Division

EFFECTS OF ISOTROPIC ALPHA POPULATIONS  
ON TOKAMAK BALLOONING STABILITY

D. A. Spong	J. J. Ramos <sup>c</sup>
D. J. Sigmar <sup>a</sup>	D. E. Hastings <sup>c</sup>
K. T. Tsang <sup>b</sup>	W. A. Cooper <sup>d</sup>

---

<sup>a</sup>Plasma Fusion Center, Massachusetts Institute of Technology, Cambridge; on leave from Oak Ridge National Laboratory.

<sup>b</sup>Plasma Research Institute, Science Applications International Corporation, Boulder, Colorado.

<sup>c</sup>Plasma Fusion Center, Massachusetts Institute of Technology, Cambridge.

<sup>d</sup>Centre des Recherches en Physique des Plasmas, CH-1007, Lausanne, Switzerland.

Date Published: December 1986

Prepared by  
OAK RIDGE NATIONAL LABORATORY  
Oak Ridge, Tennessee 37831  
operated by  
MARTIN MARIETTA ENERGY SYSTEMS, INC.  
for the  
U.S. DEPARTMENT OF ENERGY  
under contract DE-AC05-84OR21400



3 4456 0145693 2



CONTENTS

ABSTRACT.....	v
1. INTRODUCTION.....	1
2. BASIC EQUATIONS.....	5
3. NUMERICAL SOLUTION METHODS.....	24
4. DISCUSSION OF RESULTS.....	27
5. CONCLUSIONS.....	34
REFERENCES.....	36



## ABSTRACT

Fusion product alpha populations can significantly influence tokamak stability due to coupling between the trapped alpha precessional drift and the kinetic ballooning mode frequency. This effect is of particular importance in parameter regimes where the alpha pressure gradient begins to constitute a sizable fraction of the thermal plasma pressure gradient. Careful, quantitative evaluations of these effects are necessary in burning plasma devices such as the Tokamak Fusion Test Reactor and the Joint European Torus, and we have continued systematic development of such a kinetic stability model. In this model we have considered a range of different forms for the alpha distribution function and the tokamak equilibrium. Both Maxwellian and slowing-down models have been used for the alpha energy dependence while deeply trapped and, more recently, isotropic pitch angle dependences have been examined. In the latter case the drift reversal of the not so deeply trapped alphas is an important new feature not included in the deeply trapped model. The tokamak equilibrium was initially described using the nearly concentric circular flux surface model as well as more realistic analytic and numerical calculations that include the higher order poloidal harmonics of the equilibrium. An improved analytic model gives especially close agreement with the finite  $\beta$  numerical equilibrium. Detailed comparisons of these various models are presented. Our results indicate that alpha populations can significantly deteriorate the first stability window for ballooning modes as the alpha pressure gradient is increased and as the background electron temperature is raised (for the slowing-down model) or,

equivalently, the ratio of alpha to background temperature is lowered (for the Maxwellian model). A related effect is the observed destabilization with increased aspect ratio ( $\epsilon_p^{-1} = R_0/r_p$  where  $r_p$  is the local pressure gradient scale length). These scalings are consistent with an interaction between the ballooning mode frequency and the alpha precessional drift at energies involving increasingly larger fractions of the alpha distribution. Such regimes will characterize the central regions of burning tokamak devices and should be observable for the projected ranges of alpha pressure and background temperature.

## 1. INTRODUCTION

The interaction of hot particle species with tokamak stability has been of substantial interest [1-8] in recent years due to the natural occurrence of suprathreshold populations from neutral beam and rf heating and, ultimately, from alphas in ignition devices. The consequences of this interaction depend strongly on the parameter range and type of mode under consideration. An overall classification can be made in terms of the relative magnitude of the mode frequency ( $\omega$ ) relative to the hot species precessional drift frequency ( $\omega_{dH}$ ).

First, for moderately energetic populations, one has  $\omega \approx \omega_{dH}$ , which can lead to destabilizing couplings of the hot species with the kinetic ballooning mode [1,2] and with the pressure-driven internal kink [4,5]. Such interactions have been studied theoretically in some detail for the case of alpha populations in burning tokamaks and for neutral beam-generated tails in present-day devices. In the latter case, this destabilization has been verified experimentally in the form of the "fishbone oscillations" observed with near perpendicular injection on the Poloidal Divertor Experiment (PDX) [5]. Such fluctuations have components of the interaction of the trapped energetic species with internal kinks (the low frequency, low mode number oscillations) and with ballooning modes. The fishbone oscillations cause rapid loss of the fast particle component; destabilizing the ballooning mode affects the bulk plasma confinement.

Second, for very highly energetic populations (in the multi-MeV range), one has  $\omega \ll \omega_{dH}$ , which leads to a stabilizing influence on

ballooning modes [6] due to the hot species enhancement of the plasma compressibility. This effect tends to become more pronounced as the hot species pressure is increased; however, it does not rely on or require production of a diamagnetic well by the hot component. It has been proposed [6] that such an effect could be utilized to allow access between first and second stable regimes in the tokamak.

Our specific interest in this report is to examine interactions of alpha populations with ballooning modes. Slowing-down alphas in ignition-grade plasmas ( $T_{i,e} \geq 10\text{-}20$  keV) have sufficient collisional coupling to the background thermal plasma to generally reside in the moderate energy ( $\omega \approx \omega_{dH}$ ) regime. The strength of the interaction is related to the alpha pressure gradient, which can be a sizable fraction of the background plasma gradient due to the centrally peaked nature of the alpha particle source ( $\approx n^2 \langle \sigma v \rangle$ ). As shown in this report, this coupling is not always necessarily destabilizing. There are ranges of shear and pressure gradient where ballooning stability is improved; however, the first stability window, which will limit the central part of the profile, is generally always destabilized. The possible consequences of this destabilization could be a deterioration of the background plasma beta limit as well as an enhanced loss of the alpha component before thermalizing. Since either of these outcomes can seriously impair the chances for achieving ignited conditions, a careful, quantitative evaluation is called for, both in the present generation of break-even experiments and for the proposed compact ignition device. The goal of this approach is first to develop a realistic model for delineating unstable parameter regimes that should

be avoided by burning plasma devices and, ultimately, for carrying out optimization studies (with respect to cross-sectional shaping and possible tailoring of the hot distribution function) to enlarge the stable window of operation. An important reason for pursuing such optimizations is that the type of shaping required to improve stability in an alpha-dominated, burning plasma is not necessarily the same as that already developed for the background thermal plasma alone. This is due to the different weighting of the curvature by the trapped hot species from that of the usual MHD instability driving term in the ballooning equation.

We systematically develop the theory of coupling between an alpha population and the kinetic ballooning mode; we also present stability results over the parameter ranges characteristic of ignition experiments. First, the general form of the two coupled mode equations for the perturbed fields is presented, subject to a number of approximations appropriate for a trapped alpha species. Next, we choose a particular alpha distribution function and discuss the tokamak equilibrium model. Then, an approximate method for reducing the two coupled mode equations to a single equation in the case of an isotropic alpha distribution is discussed. This approach is useful in that the components of the equation which arise from the conventional ideal MHD ballooning theory can be clearly identified and separated from the new terms describing the hot species and background coupling effects. Also, the new terms appear in a fairly simple form, indicating the mechanism of the coupling. Next, we describe numerical solution techniques used to solve both the full coupled set of

integro-differential equations and the approximate single eigenmode equation limit. Finally, we present a number of numerical results for the different models using parameters relevant to ignition tokamaks and conclude by summarizing our findings and discussing their implications.

## 2. BASIC EQUATIONS

The equations developed here are based on the analysis of Ref. [9], where a general gyrokinetic formalism was used to derive a set of coupled equations describing short wavelength ballooning modes in an arbitrary geometry, including the tokamak. This work retained the hot and background species finite Larmor radius effects and evaluated the hot population response for frequencies that could be comparable with the hot particle precessional drift frequency, as well as lower frequencies. This analysis also assumes that the hot particle bounce frequency is large compared to the drift frequency. The following calculations are based on the two coupled integro-differential equations [Eqs. (11) and (12)] developed from the gyrokinetic formalism of Ref. [9]. These result from taking the  $\vec{k}_\perp \times \hat{b}$  component of Ampere's law ( $\vec{k}_\perp$  = wave vector  $\perp$  to  $\vec{B}$ ,  $\hat{b} = \vec{B}/B$ ) and from applying  $B^{-1}\hat{b} \cdot \vec{\nabla}$  to the parallel component of Ampere's law and invoking quasi-neutrality. The velocity integrals in the equations are defined as only over the trapped particle region of velocity space; the circulating particles do not contribute. We make two approximations to these equations initially. These are the neglect of  $v_{\parallel}^2$  as compared to  $v_{\perp}^2$  inside the velocity integrals (since  $v_{\parallel}^2$  is down from  $v_{\perp}^2$  by the inverse aspect ratio for the trapped region of velocity space), and we retain only the hot and background species finite Larmor radius terms as they enter in through the diamagnetic drifts, but not to higher order. These approximations are made to somewhat simplify the algebra but are not essential for the methods of solution used here, which

could be generalized to include such terms. With these points taken into account, our two coupled multiple species ballooning mode equations are

$$Q_{\parallel} = \frac{c}{\omega} (\hat{\mathbf{e}} \cdot \hat{\mathbf{k}}) \phi - \frac{4\pi M_H}{\Omega_H} \int d^3 v \frac{\mu^2 (\hat{\mathbf{e}} \cdot \vec{\nabla} F_H)}{\langle \omega_{dH} \rangle - \omega} \langle Q_{\parallel} \rangle , \quad (1)$$

$$\begin{aligned} \frac{B v_A^2}{k_{\perp}^2} \hat{\mathbf{b}} \cdot \vec{\nabla} \left( \frac{k_{\perp}^2}{B} \hat{\mathbf{b}} \cdot \vec{\nabla} \phi \right) + D_1 \phi + \frac{\omega V_A^2}{k_{\perp}^2} (\hat{\mathbf{e}} \cdot \hat{\mathbf{k}}) Q_{\parallel} \\ = \frac{4\pi M_H}{B \Omega_H} \left( \frac{\omega V_A^2}{c k_{\perp}^2} \right) (\hat{\mathbf{e}} \cdot \hat{\mathbf{k}}) \int d^3 v \frac{v_{\parallel}^2 \mu (\hat{\mathbf{e}} \cdot \vec{\nabla} F_H)}{\langle \omega_{dH} \rangle - \omega} \langle Q_{\parallel} \rangle , \end{aligned} \quad (2)$$

where

$$\hat{\mathbf{e}} = \hat{\mathbf{k}}_{\perp} \times \hat{\mathbf{b}} , \quad \hat{\mathbf{b}} = \vec{B}/B , \quad \hat{\mathbf{k}} = (\hat{\mathbf{b}} \cdot \vec{\nabla}) \hat{\mathbf{b}} ,$$

$$\hat{\mathbf{k}}_{\perp} = \vec{\nabla}(\phi - q\Theta) , \quad \Omega_H = \frac{Z_H e B}{M_H C} ,$$

$$D_1 = \omega^2 - \omega \omega_p + \frac{\omega_{\kappa}(\omega_{\perp} + \omega_{\parallel})}{b} - \frac{2\omega_{\kappa}^2}{b\beta} ,$$

$$\langle \omega_{dH} \rangle = \frac{B}{\Omega_H} \langle B^{-1} \hat{\mathbf{k}}_{\perp} \times \hat{\mathbf{b}} \cdot (\mu \vec{\nabla} B + v_{\parallel}^2 \hat{\mathbf{k}}) \rangle ,$$

$$\langle \dots \rangle = \frac{\int \frac{d\mathbf{l}}{v_{\parallel}} (\dots)}{\int \frac{d\mathbf{l}}{v_{\parallel}}} ,$$

$$\omega_p = \rho^{-1} \left( \sum_j \hat{\mathbf{e}} \cdot \vec{\nabla} p_{\perp j} / \Omega_j \right) ,$$

$$\omega_{\parallel, \perp} = \rho^{-1} \left( \sum_j \Omega_j^{-1} \right) \vec{e} \cdot \vec{\nabla} p_{\parallel, \perp} ,$$

$$b = \rho^{-1} k_{\perp}^2 \left( \sum_j \Omega_j^{-1} \right) \sum_j (p_{\perp j} / \Omega_j) ,$$

$$\hat{\beta} = \frac{8\pi}{B^2} \left[ \sum_j (p_{\perp j} / \Omega_j) \right] / \left( \sum_j \Omega_j^{-1} \right) ,$$

$\phi$  = perturbed potential ,

$$Q_{\parallel} = \frac{\omega}{c} \tilde{B}_{\parallel} + (\vec{e} \cdot \vec{\nabla} B) B^{-1} \phi$$

= Lagrangian magnetic field perturbation

parallel to  $\vec{B}$  (equilibrium) .

The distribution function  $F_H$  must depend only on the constants of the motion,  $E$  and  $\mu$ . For the purposes of this report, we break it up into a pitch angle-dependent part  $F_{\lambda}$  and an energy-dependent part  $F_E$ . For  $F_E$  we use a slowing-down distribution with a cutoff at the alpha birth energy,  $E_{\alpha}$ , as the most appropriate model for alphas in ignited plasmas.

$$F_H(E, \mu) = F_E F_{\lambda} , \tag{3}$$

with

$$F_E = \begin{cases} \frac{3N_H}{4\pi \ln(1 + \delta^{-3})(v^3 + v_c^3)} & v < v_\alpha , \\ 0 & v \geq v_\alpha , \end{cases}$$

$$v_\alpha = \sqrt{2E_\alpha/M_H} ,$$

$$v_c = 3\sqrt{\pi} \frac{M_e}{M_H} [Z] (2T_e/M_e)^{3/2} ,$$

$$\delta = v_c/v_\alpha \quad (\text{assumed here to be radially constant}) ,$$

$$[Z] = \sum_{\text{ions}} \frac{Z_i^2 n_i / A_i}{n_e} ,$$

$A_i$  = atomic mass number ,

$Z_i$  = charge number ,

$n_e, T_e, M_e$  = background plasma electron density,

temperature, and mass ,

$F_\lambda$  = a function of  $\lambda$  ( $\lambda = \mu B_{\min}/E$ ) subject to the normalization:

$$\int_0^{2\pi} d\theta \left( \frac{B}{\pi B_{\min}} \right) \int_0^{M^{-1}} \frac{d\lambda F_\lambda}{(1 - \lambda M)^{1/2}} = 1 ,$$

where  $M_0 = B_{\max}/B_{\min}$  and  $M = B/B_{\min}$  ,

$B_{\max}, B_{\min}$  = maximum and minimum magnetic

field on flux surface of interest .

For the results given in this report, the isotropic limit  $F_\lambda = 1$  will be taken. This is motivated by the fact that alphas are born isotropically. However, we retain  $F_\lambda$  in the analysis through the next set of equations since it may be of interest at some point to consider nonuniform  $F_\lambda$ 's as would be formed by a possible anisotropic loss mechanism (e.g., fishbone losses) of the alpha losses during slowing down. If we now substitute Eq. (1) for the  $Q_{||}$  term occurring on the left-hand side of Eq. (2) and use the above distribution function in the velocity integrals, the following system of equations results:

$$Q_{||} = \frac{c}{\omega} (\vec{e} \cdot \vec{\kappa}) \phi - \frac{3\pi M_H M (\vec{e} \cdot \vec{\nabla} N_H) v_c^4}{2 \ln(1 + \delta^{-3}) B_{\min}^2 \omega_{do} \Omega_H} I_1(\Theta) , \quad (4)$$

$$\begin{aligned} & \frac{B v_A^2}{k_{||}^2} \hat{b} \cdot \vec{\nabla} \left( \frac{k_{||}^2}{B} \hat{b} \cdot \vec{\nabla} \phi \right) + \left[ D_1 + \frac{v_A^2}{k_{||}^2} (\vec{e} \cdot \vec{\kappa})^2 \right] \phi \\ & = \left( \frac{\omega v_A^2}{c k_{||}^2} \right) \frac{3\pi M_H M v_c^4 (\vec{e} \cdot \vec{\nabla} N_H) (\vec{e} \cdot \vec{\kappa})}{2 B_{\min} \omega_{do} B \Omega_H \ln(1 + \delta^{-3})} I_2(\Theta) , \end{aligned} \quad (5)$$

where

$$I_1(\Theta) = \int_{M_0^{-1}}^{M^{-1}} \frac{d\lambda F_\lambda \lambda^2 \langle Q_{||} \rangle}{(1 - \lambda M)^{1/2}} H(\eta, \delta, \lambda) ,$$

$$I_2(\Theta) = \int_{M_0^{-1}}^{M^{-1}} \frac{d\lambda \lambda F_\lambda (2 - \lambda M) \langle Q_{||} \rangle}{(1 - \lambda M)^{1/2}} H(\eta, \delta, \lambda) ,$$

$$H(\eta, \delta, \lambda) = \int_0^{\delta^{-1}} \frac{x^6 dx}{(1 + x^3) [x^2 \tilde{F}_d(\lambda) - \eta]} ,$$

$$\eta = \eta_0 \Omega, \quad \Omega = \omega/\omega_A, \quad x = v/v_c,$$

$$\omega_A = v_A/qR_0,$$

$$\tilde{f}_d(\lambda) = f_d(\lambda)/f_{d1}, \quad f_{d1} = f_d(\lambda=1),$$

$$f_d(\lambda) = \frac{rR_0}{q} \langle B^{-1} \vec{e} \cdot \left[ -\frac{\lambda}{B} \vec{\nabla}(p_c + p_{\perp\alpha}) + (2B_{\min} - \lambda B) \vec{\kappa} \right] \rangle,$$

$$\omega_{do} = \frac{qv_c^2}{2rR_0} \Omega_H M f_{d1},$$

$$\eta_0 = \frac{2\omega_A}{Bv_c^2 f_{d1}},$$

$R_0$  = radius of the magnetic axis ,

$r$  = average minor radius of the flux surface.

Here we have used the equilibrium force balance relation to express  $\vec{\nabla}B$  in terms of  $\vec{\nabla}p$  and  $\vec{\kappa}$  in the drift frequency function  $f_d(\lambda)$ .

As written, Eqs. (4) and (5) are valid for arbitrary equilibria. We have considered several different toroidal equilibrium models in solving these equations: (a) the shifted circular flux surface model [10], (b) an improved shifted circular flux surface model of Ref. [11] which more accurately treats the radial variation and first derivative

of the shift, and (c) a general numerical two-dimensional toroidal equilibrium. In all cases we use the isotropic limit for the alpha population ( $F_\lambda = 1$ ) so that only a scalar pressure toroidal equilibrium need be considered in which the alpha pressure is simply additive to the background plasma pressure.

These equilibria are all based upon the ballooning transformation [10] which maps  $\theta$  from the interval  $-\pi \leq \theta \leq \pi$  to the extended infinite interval  $-\infty \leq \theta \leq \infty$  subject to the boundary conditions that  $\phi$  and  $Q_{||}$  vanish at  $\theta = \pm\infty$ . The effect of this transformation on Eqs. (4) and (5) is that all functions of  $\theta$  are mapped onto the infinite interval. The bounce averages appearing inside the integrals  $I_1$  and  $I_2$  are performed over the appropriate  $\lambda$ -dependent subintervals of the same  $2\pi$  interval at which the other (nonintegral) terms of Eqs. (4) and (5) are being evaluated.

Although the numerical equilibrium is ultimately the most realistic of the three models and is best for careful quantitative stability studies, the analytic models (a) and (b) are useful for parameter sensitivity studies of the effects of hot populations on ballooning modes. These models have the virtue of allowing stability results to be characterized in terms of a few simple dimensionless parameters descriptive of a single flux surface. The relevant terms in Eqs. (4) and (5) which must be provided by the equilibrium model are  $k_{\perp}^2$ ,  $\vec{k}_{\perp} \times \hat{b} \cdot \vec{\nabla} p$ ,  $\vec{k}_{\perp} \times \hat{b} \cdot \vec{\kappa}$ , and  $\hat{b} \cdot \vec{\nabla}$ . It is a well-known consequence of the ballooning transformation that certain of these terms do not remain purely periodic, but contain secular (i.e., proportional to  $\theta$  or  $\theta^2$ ) dependences. We explicitly indicate this by writing them in the form

$$k_{\perp}^2 = k_{\perp 0}^2 + k_{\perp 1}^2 \theta + k_{\perp 2}^2 \theta^2 , \quad (6)$$

$$\vec{k}_{\perp} \times \hat{b} \cdot \vec{\kappa} = (\vec{k}_{\perp} \times \hat{b} \cdot \vec{\kappa})_0 + (\vec{k}_{\perp} \times \hat{b} \cdot \vec{\kappa})_1 \theta , \quad (7)$$

$$\vec{k}_{\perp} \times \hat{b} \cdot \vec{\nabla} p = (\vec{k}_{\perp} \times \hat{b} \cdot \vec{\nabla} p)_0 , \quad (8)$$

where each of the coefficients  $k_{\perp 0}^2$ ,  $k_{\perp 1}^2$ ,  $k_{\perp 2}^2$ ,  $(\vec{k}_{\perp} \times \hat{b} \cdot \vec{\nabla} p)_0$ , and  $(\vec{k}_{\perp} \times \hat{b} \cdot \vec{\kappa})_{0,1}$  is now periodic in  $\theta$ . The results of the equilibrium of Ref. [11] for an isotropic plasma are then as follows:

$$k_{\perp 0}^2 = \frac{q^2 D^2}{r^2} (1 + h_0^2) , \quad (9)$$

$$k_{\perp 1}^2 = 2 \frac{q^2 D^2}{r^2} h_0 h_1 , \quad (10)$$

$$k_{\perp 2}^2 = \frac{q^2 D^2}{r^2} , \quad (11)$$

$$(\vec{k}_{\perp} \times \hat{b} \cdot \vec{\kappa})_0 = \frac{qD}{rR_0} (\cos\theta + h_0 \sin\theta) , \quad (12)$$

$$(\vec{k}_{\perp} \times \hat{b} \cdot \vec{\kappa})_1 = \frac{qD}{rR_0} h_1 \sin\theta , \quad (13)$$

$$(\vec{k}_{\perp} \times \hat{b} \cdot \vec{\nabla} p)_0 = \frac{\alpha B^2}{8\pi r R_0 q} , \quad (14)$$

$$\hat{b} \cdot \vec{\nabla} = \frac{1}{R_0 q D} \frac{d}{d\theta} , \quad (15)$$

where

$$h_0 = \frac{1}{D^2} \left[ \frac{\tilde{\delta}^2}{2} \sin 2\theta - (\tilde{\delta} + \tilde{\delta}_s + r\tilde{\delta}') \sin\theta \right] ,$$

$$h_1 = s/D^2 ,$$

$$D = 1 - \tilde{\delta} \cos\theta ,$$

$$\tilde{\delta} = \left\{ 1 - \frac{2}{\sqrt{3}\lambda_p} \sinh \left[ \frac{1}{3} \sinh^{-1} \frac{3\sqrt{3}\lambda_p}{2} \right] \right\}^{1/2} ,$$

$$r\tilde{\delta}' = \frac{(1 - \tilde{\delta}^2)}{(1 + 2\tilde{\delta}^2)} \left[ (1 - \tilde{\delta}^2)^{3/2} \alpha + (2s - 3)\tilde{\delta} \right] ,$$

$$s = \frac{rq'}{q} , \quad \alpha = - \frac{8\pi q^2 R_0 p'}{B^2} , \quad q = \frac{rB_t}{R_0 B_p} ,$$

$$\lambda_p = - \frac{2q^2 R_0}{B_0^2 r^3} \int_0^r \frac{dp}{dr} r^2 dr \approx \frac{\alpha}{4} \quad (\text{for a parabolic } p \text{ profile}) .$$

These results will reduce to the limit considered in Ref. [10] if we take  $\lambda_p \rightarrow 0$ . This results in  $\tilde{\delta} \rightarrow 0$ ,  $r\tilde{\delta}' \rightarrow \alpha$ , and  $D \rightarrow 1$ . The difference in the two models is that the above more accurately retains the finite shift of the flux surfaces and more accurately treats the radial dependence of the shift. Also, the earlier model [10] assumes a low  $\beta_p$  pressure profile that has a steep slope through the flux surface of interest, whereas the above approximation [11] allows the radial variation of the pressure to be more gradual (due to the finiteness of the  $\lambda_p$  parameter). Finally, the above model retains  $\sin 2\theta$  terms as well as  $\sin\theta$ . This model has been generalized to include an anisotropic hot population with arbitrary  $p_\perp$  profile. Although we will

not repeat the specific details here, such an equilibrium is useful, for example, in carrying out the deeply trapped limit [1,8] of the hot species ballooning mode equations.

The accuracy of these models can be examined by comparing the periodic coefficients of Eqs. (9) - (15) with results for the same terms calculated using the numerical equilibrium. For this, we have used the MOMCON equilibrium code described in Ref. [12] as applied to an axisymmetric tokamak. The results of the equilibrium are then mapped to a straight field line coordinate system and the quantities in Eqs. (9) - (15) calculated. Although an exact comparison of the numerical and analytic equilibrium results is not possible (since quantities such as  $\alpha$  will vary around the flux surface in the numerical calculation), we have calculated flux surface averages of such parameters in order to do an approximate benchmark of the different models. The results of this are shown in Fig. 1, where the two analytic calculations along with the numerical results are displayed. As may be seen, the coefficients given by Ref. [11] are generally closer to the numerical calculation than those of Ref. [10], as might be expected, due to the retention of higher order effects in this model. Examination of such plots over a range of differing  $\beta$  values and aspect ratios has led us to conclude that the results given in Eqs. (9) - (15) should provide an equilibrium of reasonable accuracy for parameters relevant to break-even conditions in circular tokamaks. The exact numerical equilibrium also has been coupled to the stability codes discussed here and will be of particular importance for studies of the effects of alpha populations on ballooning in noncircular tokamaks.

ORNL-DWG 86-2474R FED

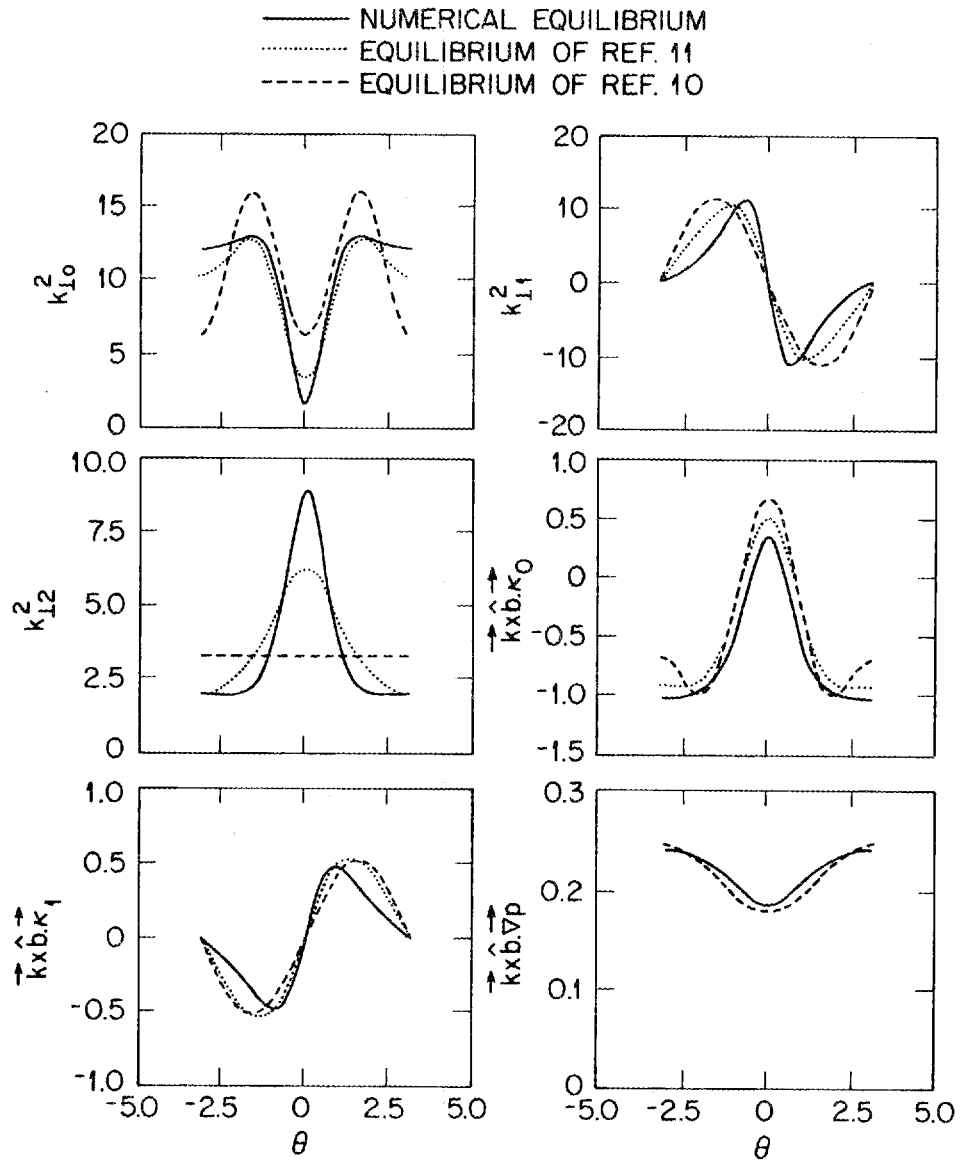


Fig. 1. Comparison of periodic equilibrium coefficients entering the ballooning equation based on a numerical equilibrium calculation (solid line), the analytic equilibrium of Ref. [10] (dashed line), and the equilibrium of Ref. [11] (dotted line).

One further equilibrium quantity of interest which has been calculated is the bounce-averaged drift frequency  $\langle\omega_{dH}\rangle$ . This was given following Eqs. (4) and (5) [i.e., the  $f_d(\lambda)$  function] and is important in determining the degree of coupling present between the alpha component and background plasma modes. A typical example of  $\langle\omega_{dH}\rangle$  is shown in Fig. 2, where it is plotted vs  $\lambda$  ( $= \mu B_{\min}/E$ ) for a number of differing  $\beta$ 's for an aspect ratio of 3.5. Here  $\beta_\psi$  is the total (alpha plus background) local beta on the flux surface where the calculation is carried out. The dashed line on the left-hand side is the trapped-passing boundary ( $\lambda = B_{\min}/B_{\max}$ ) where the alpha banana

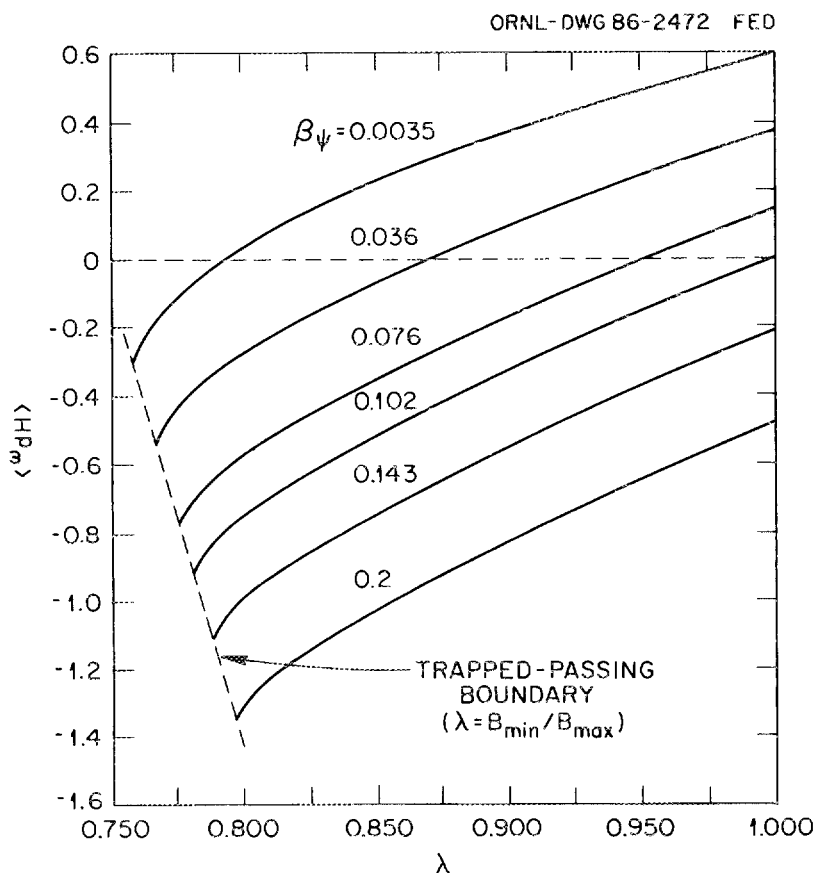


Fig. 2. Bounce-averaged trapped particle drift frequency as a function of  $\lambda$  and the local  $\beta$ .

orbits extend all the way to the inside of the torus and average over both good and bad curvature, thus lowering  $\langle \omega_{dH} \rangle$  to negative values. The trapped-passing boundary is not a vertical line since the value of  $B_{\min}/B_{\max}$  shifts upward as the  $\beta$  of the equilibrium is raised. On the right-hand side is the deeply trapped limit at  $\lambda = 1$ , where the alphas sample only unfavorable curvature and have  $\langle \omega_{dH} \rangle > 0$ , except at the higher  $\beta$ 's. As  $\beta$  is raised, the plasma diamagnetism begins to modify the gradient of B enough to overcome the curvature term and reverse the drift frequency at increasingly higher values of  $\lambda$ . This happens on the average at about  $\beta = 5\%$  in Fig. 2, and the deeply trapped value of  $\langle \omega_{dH} \rangle$  reverses at  $\beta \approx 10\%$ .

Substituting the equilibrium given in Eqs. (9) - (15) into Eqs. (4) and (5) leads to the following coupled system. Here we have defined a new variable  $\tilde{Q}_{\parallel}$  which differs from  $Q_{\parallel}$  by a factor that is independent of  $\theta$ ; this is for convenience to avoid unnecessary dimensional factors in the final equations.

With

$$\tilde{Q}_{\parallel} = \frac{r\Omega}{q^2} \left( \frac{V_A}{c} \right) Q_{\parallel} ,$$

$$\tilde{Q}_{\parallel} = D(\cos\theta + h\sin\theta)\phi - \frac{\alpha_H (B_0/B_{\min})^2 \delta^2 \tilde{I}_1(\theta)}{2q^2 f_0(\delta) f_{d1} \ln(1 + \delta^{-3})} , \quad (16)$$

$$\begin{aligned} \frac{d}{d\theta} \left[ D(1 + h^2) \frac{d\phi}{d\theta} \right] + \left[ \Omega(\Omega - \Omega_p) D^3 (1 + h^2) + D^2 (\cos\theta + h\sin\theta) (\alpha_c + \alpha_H) \right] \phi \\ = \left( \frac{B_0^2}{BB_{\min}} \right) \frac{\alpha_H \delta^2 D^2 (\cos\theta + h\sin\theta)}{2f_{d1} f_0(\delta) \ln(1 + \delta^{-3})} \tilde{I}_2(\theta) , \end{aligned} \quad (17)$$

and  $\tilde{I}_1, \tilde{I}_2$  are defined as before [following Eq. (5)] except with  $\tilde{Q}_{||}$  in the integrand.

Equations (16) and (17) now can be solved either directly using an iterative numerical approach (as will be discussed later) or by first approximating the integrals (based on the expected shape of the  $\tilde{Q}_{||}$  function). The latter approach is useful in that it leads to a single integro-differential equation involving only  $\phi$ ; this equation can be solved exactly for  $\phi$ , and iterations are only required to obtain the eigenvalue  $\Omega$  (as determined by the boundary condition imposed on  $\phi$  at  $\theta = 0$ ). This solution can then be used as an initial guess for the iterative solution of the full coupled Eqs. (16) and (17) which will involve numerical iterations to obtain  $\phi$  and  $\tilde{Q}_{||}$  in addition to those required for  $\Omega$ .

The approximate approach relies on the fact that  $\tilde{Q}_{||}$  is typically highly peaked about  $\theta = 0$ . This characteristic shape then implies that bounce averages of  $\tilde{Q}_{||}$  which enter in the integrals  $I_1$  and  $I_2$  will be peaked about  $\lambda = 1$ ; such a dependence is generally seen in the numerical solutions and is especially apparent in bounce averages over the lowest interval  $-\pi \leq \theta \leq \pi$ . As a result, one can approximate  $\tilde{I}_1$  and  $\tilde{I}_2$  by removing the more slowly varying components of their integrands (evaluated at  $\lambda = 1$ ) outside the integral and retaining the more rapidly varying components  $\tilde{Q}_{||}$  and  $(1 - \lambda M)^{-1/2}$  inside, as indicated here:

$$\tilde{I}_1 = [\lambda^2 H(\eta, \delta, \lambda)]_{\lambda=1} I_0(\theta) , \quad (18)$$

$$\tilde{I}_2 = [(2 - \lambda M) H(\eta, \delta, \lambda)]_{\lambda=1} I_0(\theta) , \quad (19)$$

with

$$I_0(\theta) = \int_{M_0^{-1}}^{M^{-1}} \frac{d\lambda \langle \tilde{Q}_{||} \rangle}{(1 - \lambda M)^{1/2}} .$$

This approach can be thought of as an application of the mean value theorem justified a posteriori by iteration. In effect, we have chosen  $\lambda^* = 1$  as a first approximation to the integral. A somewhat improved approximation [which still permits Eqs. (16) and (17) to be decoupled] is also possible if one retains the  $H(\eta, \delta, \lambda)$  function inside the  $I_0(\theta)$  integral.

We are then left with the single  $\lambda$  integral,  $I_0$  of Eqs. (18) and (19). The fact that the upper limit of this integrand ( $M^{-1} = B/B_{\min}$ ) depends on  $\theta$ , however, would still prevent one from reducing Eqs. (16) and (17) to a single equation for  $\phi$ . To make further progress, we then note that the assumption that  $\langle Q_{||} \rangle$  is peaked about  $\lambda = 1$  implies that  $I_0$  is peaked about  $\theta = 2m\pi$ ,  $m = 0, 1, 2, \dots$  (i.e., at which  $M^{-1} = 1$ ). The height of this peak is simply  $I_0(\theta = 0)$ . The  $I_0$  integral then clearly has two characteristics: it is peaked at  $\theta = 0$ , and it vanishes smoothly to 0 at  $\theta = (2m + 1)\pi$  due to the fact that the upper and lower limits coalesce ( $M^{-1} \rightarrow M_0^{-1}$ ) at these points. A reasonable approximation to  $I_0$  then is to use its peak value multiplied by a function that is 1 at  $\theta = 2m\pi$  and 0 at  $\theta = (2m + 1)\pi$ :

$$I_0(\theta) \approx K(\theta) \int_{M_0^{-1}}^1 \frac{d\lambda \langle \tilde{Q}_{||} \rangle}{(1 - \lambda)^{1/2}} ,$$

with

$$K(\theta) = \begin{cases} 1 & \text{at } \theta = 2m\pi, \\ 0 & \text{at } \theta = (2m + 1)\pi, \\ & m = 0, 1, 2, \dots \end{cases}$$

The structure of  $I_0(\theta)$  then leads us to choose the following form for  $K(\theta)$ :

$$K(\theta) = \frac{\int_{M_0^{-1}}^{M^{-1}} \frac{d\lambda}{(1 - \lambda M)^{1/2}}}{\int_{M_0^{-1}}^1 \frac{d\lambda}{(1 - \lambda)^{1/2}}} = \frac{(1 - M/M_0)^{1/2}}{M(1 - M_0^{-1})^{1/2}},$$

which goes to the above-mentioned limits. Our resulting final approximation to  $\tilde{I}_1$  and  $\tilde{I}_2$  will then be denoted by

$$\tilde{I}_1(\theta) \approx \frac{2}{M} \left(1 - \frac{M}{M_0}\right)^{1/2} H(\eta, \delta) \langle \overline{\tilde{Q}_{\parallel}} \rangle, \quad (20)$$

$$\tilde{I}_2(\theta) \approx \frac{2}{M} (2 - M) \left(1 - \frac{M}{M_0}\right)^{1/2} H(\eta, \delta) \langle \overline{\tilde{Q}_{\parallel}} \rangle, \quad (21)$$

where  $H(\eta, \delta)$  is the integral:

$$H(\eta, \delta) = \int_0^{\delta^{-1}} \frac{x^6 dx}{(1 + x^3)(x^2 - \eta)},$$

i.e.,  $H(\eta, \delta)$  is  $H(\eta, \delta, \lambda)$  evaluated at  $\lambda = 1$ ,

and the pitch angle averaging operator  $\langle \overline{\dots} \rangle$  is defined by

$$\langle \overline{\dots} \rangle = \frac{\int_{M_0^{-1}}^1 \frac{d\lambda \langle \dots \rangle}{(1 - \lambda)^{1/2}}}{\int_{M_0^{-1}}^1 \frac{d\lambda}{(1 - \lambda)^{1/2}}} = \int_{M_0^{-1}}^1 \frac{d\lambda \langle \dots \rangle}{2(1 - M_0^{-1})^{1/2}} .$$

It may be noted that the above operator first transforms a function of  $\theta$  (such as  $\tilde{Q}_{\parallel}$ ) into a function of  $\lambda$  and then transforms this into a single number; this characteristic is necessary in order to decouple Eqs. (16) and (17). The  $\lambda$  dependence enters through the integration boundaries of the bounce-averaging operator  $\langle \rangle$ .

Equation (16) may now be written approximately as

$$\begin{aligned} \tilde{Q}_{\parallel} &= D(\cos\theta + h\sin\theta)\phi \\ &- \frac{\alpha_H (B_0/B_{\min})^2 \delta^2}{q^2 f_0(\delta) f_{d1} \ln(1 + \delta^{-3})} \left(\frac{B_{\min}}{B}\right) \left(1 - \frac{B}{B_{\max}}\right)^{1/2} H(\eta, \delta) \langle \overline{\tilde{Q}_{\parallel}} \rangle . \end{aligned} \quad (22)$$

This is solved simply by operating on it with  $\langle \overline{\dots} \rangle$  to obtain

$$\begin{aligned} \langle \overline{\tilde{Q}_{\parallel}} \rangle &= \frac{q^2 f_0(\delta) f_{d1} \ln(1 + \delta^{-3}) \langle \overline{D(\cos\theta + h\sin\theta)\phi} \rangle}{q^2 f_0(\delta) f_{d1} \ln(1 + \delta^{-3}) + \alpha_H \delta^2 H(\eta, \delta) \left\langle \frac{B_0^2}{BB_{\min}} \left(1 - \frac{B}{B_{\max}}\right)^{1/2} \right\rangle} . \end{aligned} \quad (23)$$

Substituting this back into Eq. (22) then leads to

$$\tilde{Q}_{\parallel} = D(\cos\theta + h\sin\theta)\phi$$

$$\frac{\alpha_H \delta^2 \left( \frac{B_0}{B_{\min}} \right) (1 - B/B_{\max})^{1/2} \langle D(\cos\theta + h\sin\theta)\phi \rangle H(\eta, \delta)}{q^2 f_0(\delta) f_{d1} \ln(1 + \delta^{-3}) + \alpha_H \delta^2 \left\langle \frac{B_0^2}{B_{\min}} \left( 1 - \frac{B}{B_{\max}} \right)^{1/2} \right\rangle H(\eta, \delta)} . \quad (24)$$

The approximate version of Eq. (17) is

$$\begin{aligned} & \frac{d}{d\theta} \left[ D(1 + h^2) \frac{d\phi}{d\theta} \right] + \left[ \Omega(\Omega - \Omega_p) D^3 (1 + h^2) + D^2 (\cos\theta + h\sin\theta) (\alpha_c + \alpha_H) \right] \phi \\ & = \alpha_H \left( \frac{B_0}{B} \right)^2 \frac{\delta^2 D^2 (\cos\theta + h\sin\theta)}{f_{d1} f_0(\delta) \ln(1 + \delta^{-3})} \left( 2 - \frac{B}{B_{\min}} \right) \left( 1 - \frac{B}{B_{\max}} \right)^{1/2} H(\eta, \delta) \langle \tilde{Q}_{\parallel} \rangle . \quad (25) \end{aligned}$$

Substituting  $\langle \tilde{Q}_{\parallel} \rangle$  from Eq. (23) into the right-hand side then leads to a single ballooning mode equation for  $\phi$ :

$$\begin{aligned} & \frac{d}{d\theta} \left[ D(1 + h^2) \frac{d\phi}{d\theta} \right] + \left[ \Omega(\Omega - \Omega_p) D^3 (1 + h^2) + D^2 (\cos\theta + h\sin\theta) (\alpha_c + \alpha_H) \right] \phi \\ & = \alpha_H G(\theta) \langle D(\cos\theta + h\sin\theta)\phi \rangle , \quad (26) \end{aligned}$$

where

$$\begin{aligned} G(\theta) = & \frac{\alpha_H D^2 \left( 2 - \frac{B}{B_{\min}} \right) \left( \frac{B_0}{B} \right)^2 \left( 1 - \frac{B}{B_{\max}} \right)^{1/2} (\cos\theta + h\sin\theta) H(\eta, \delta)}{\delta^{-2} f_0(\delta) f_{d1} \ln(1 + \delta^{-3}) + \frac{\alpha_H}{q^2} \left( \frac{B_0}{B_{\min}} \right) \left\langle \frac{B_0}{B} \left( 1 - \frac{B}{B_{\max}} \right)^{1/2} \right\rangle H(\eta, \delta)} . \end{aligned}$$

This equation consists of a differential operator on the left-hand side and an integral term on the right-hand side. The differential operator can be identified as the usual ideal ballooning MHD operator with the alpha pressure gradient augmenting the background pressure gradient in the usual MHD ballooning drive [i.e., the  $(\cos\theta + h\sin\theta)(\alpha_c + \alpha_H)$  term]. The right-hand side contains the effect of the precessional drift coupling between the thermal background and alpha species which enters in through the  $H(\eta, \delta)$  functions. The resonance in the integrand of these functions which occurs at  $\omega = \langle \omega_{dH} \rangle$  (i.e.,  $\eta = x^2$ ) will especially enhance the size of this coupling term when the mode frequency is near the precessional drift frequency of the bulk hot population. It can also be seen that the strength of the hot species response is proportional to the  $\overline{\langle \rangle}$  average of the curvature times the perturbed potential function  $\phi$  [the  $\overline{\langle D(\cos\theta + h\sin\theta)\phi \rangle}$  term]. Since  $\phi$  is typically peaked about  $\theta = 0$ , this average tends to emphasize the bad curvature region. This characteristic has been the basis of previous calculations [1, 8] using the deeply trapped approximation in which the bounce average on the right-hand side was evaluated only at  $\theta = 0$ .

### 3. NUMERICAL SOLUTION METHODS

The equations developed in the previous section have been solved numerically using techniques that we briefly describe here. To reiterate, the full coupled integro-differential system consists of Eqs. (16) and (17), and the approximation to this is Eq. (26). Equation (26) can be solved in one pass of an ordinary differential equation solver for  $\phi$ , followed by iterations for the correct  $\Omega$ . This eigenvalue is determined by requiring  $\phi$  to satisfy prescribed boundary conditions ( $d\phi/d\theta = 0$  at  $\theta = 0$ ). Solution of Eqs. (16) and (17) involves both iterations to obtain  $\phi$  and  $Q_{||}$  as well as an inner set of iterations to obtain  $\Omega$ .

We first outline the steps involved in solving the approximate Eq. (26) since its solution often provides a reasonable estimate of stability as well as being useful as a first guess for the more exact Eqs. (16) and (17). Equation (26) is a single integro-differential equation of a form that is relatively easy to solve using the same methods used in Ref. [6]. We may write this as follows:

$$\frac{d}{d\theta} \left[ A(\theta) \frac{d\phi}{d\theta} \right] + B(\Omega, \theta)\phi = E(\Omega, \theta) \langle \overline{F(\theta)\phi} \rangle . \quad (27)$$

As was pointed out in Ref. [6],  $\phi$  may be treated as a superposition of a homogeneous solution  $\phi_0$  and an inhomogeneous solution  $\phi_1$  (i.e.,  $\phi = \phi_0 + c\phi_1$ ) where these components satisfy the following equations:

$$\frac{d}{d\theta} \left( A \frac{d\phi_0}{d\theta} \right) + B\phi_0 = 0 , \quad (28)$$

$$\frac{d}{d\theta} \left( A \frac{d\phi_1}{d\theta} \right) + B\phi_1 = E(\Omega, \theta) . \quad (29)$$

Substituting  $\phi = \phi_0 + c\phi_1$  back into the original Eq. (27) then results in the following expression for the coefficient  $c$ :

$$c = \frac{\langle \overline{F\phi_0} \rangle}{1 - \langle \overline{F\phi_1} \rangle} . \quad (30)$$

This coefficient will be different for each  $2\pi$  interval in  $\theta$ , the extended ballooning variable, since the bounce averages entering into  $c$  will act only over the  $2\pi$  interval within which Eqs. (28) and (29) are currently being solved.

The solution procedure consists of solving Eqs. (28) and (29) with an initial guess for  $\Omega$  using an ordinary differential equation (o.d.e.) integrator. This is started at a sufficiently large value of  $\theta$  (we have typically used  $\theta = 5\pi$  for the calculations in this paper). The initial conditions on  $\phi_1$  are that its value and derivative are 0 at  $\theta = \theta_{\max}$ . Those for  $\phi_0$  are that its value and derivative match onto the analytic large  $s\theta$  solution of Eq. (28) which evanesces at large  $\theta$ . These two equations are then integrated over a  $2\pi$  interval. At this point,  $\phi_0$  and  $\phi_1$  are used to construct  $c$  as given above. The o.d.e. integrator is then restarted with the initial conditions that  $\phi_0$  equals  $\phi_0 + c\phi_1$  from the end of the previous  $2\pi$  interval and  $\phi_0'$  equals  $\phi_0' + c\phi_1'$ , also from the end of the previous interval. Again, the initial

conditions on  $\phi_1$  are that its value and derivative are zero. The o.d.e. integrator is then run for another  $2\pi$  interval, new starting conditions are calculated for  $\phi_0$  and  $\phi_1$ , and so on. This procedure ensures that the total solution  $\phi = \phi_0 + c\phi_1$  remains continuous from one interval to the next. For the final interval from  $\pi$  to 0, the solution is started in a similar way and stopped at  $\theta = 0$ . The total solution  $\phi$  is reconstructed, and its derivative is used as input to a root-finding routine. This routine then makes repeated adjustments in  $\Omega$  in order to annihilate the derivative of  $\phi$  at  $\theta = 0$  within some prescribed level of accuracy. For each new guess of  $\Omega$  the above process is repeated to recalculate  $\phi$ .

Solution of the full integral Eqs. (16) and (17) is done iteratively. First, the solution for  $\phi$  from Eq. (26) is substituted into Eq. (24) to calculate  $Q_{||}$ . This is then bounce averaged, resulting in a function of  $\lambda$ . From this, the integrals  $\tilde{I}_1$  and  $\tilde{I}_2$  are calculated numerically, retaining the full  $\lambda$  dependence in all components of the integrands. Equation (17) is then solved for  $\phi$  and  $\Omega$ , keeping the right-hand side fixed. Using  $\tilde{I}_1$  with this new  $\phi$  and  $\Omega$ ,  $\tilde{Q}_{||}$  is recalculated from Eq. (16). The  $\tilde{I}_1$  and  $\tilde{I}_2$  integrals are again computed using the new  $\tilde{Q}_{||}$ , Eq. (17) is solved for  $\phi$  and  $\Omega$ , a new  $\tilde{Q}_{||}$  is obtained from Eq. (16), etc. This procedure is repeated until  $\Omega$  is sufficiently converged.

## 4. DISCUSSION OF RESULTS

The effects of alpha populations on tokamak ballooning stability have been examined for a range of parameters that should characterize break-even and ignition experiments. The pressure gradient ratio  $\alpha_H/\alpha_C$  has been varied over the range from 0 to 0.5 and the background electron temperature  $T_e$  from 10 to 40 keV. The background ion temperature has been chosen as equal to  $T_e$ . The form of the alpha distribution is determined by prescribing  $\alpha_H$  and the parameter  $\delta$ , which depends only on  $T_e$ . Other parameters entering these calculations and their values are  $b_i = k^2 \rho_i^2 / 2 = 0.04$ ,  $q = 1.7$  to  $2$ ,  $R/a = 3.5$ ,  $R/r_p = 6$  ( $r_p$  = pressure gradient scale length). This value of  $R/r_p$  has been chosen to account for alpha heating in the center of the plasma, which can lead to a steeper pressure gradient than would be given by using the simple geometric aspect ratio. Since the case of alphas in a deuterium plasma is of interest, we have chosen  $Z_H/Z_i = 2$  and  $M_H/M_i = 2$ .

The numerical solution procedures described in Sec. 3 can be applied either for calculating the real and imaginary parts of  $\Omega$  with all parameters held fixed or for following marginal stability boundaries. In the latter case, the real part of  $\Omega$  and some other parameter (usually either  $s$  or  $\alpha_C$ ) are solved for, subject to the constraint that  $\Omega_i/\Omega_r$  is a small number (typically taken to be 0.05 here).  $\Omega_i/\Omega_r$  is kept finite and positive since the large  $s\theta$  boundary conditions applied to  $\phi$  at  $\theta = \theta_{\max}$  are based upon the assumption of an unstable mode. The results presented below in Figs. 3 through 6 are based on solutions of the approximate isotropic Eq. (26). The

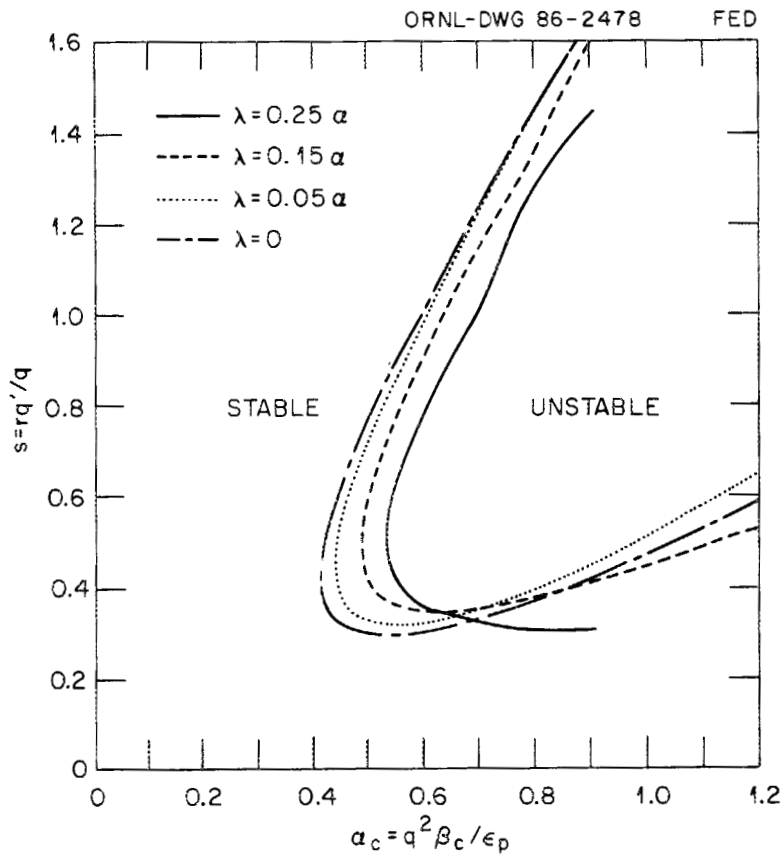


Fig. 3. Marginal stability boundaries for  $\lambda_p/\alpha = 0, 0.05, 0.1, 0.15,$  and  $0.25$  with  $\alpha_H/\alpha_c = 0.3, T_e = 20 \text{ keV}, b_i = 0.04,$  and  $q = 1.7.$

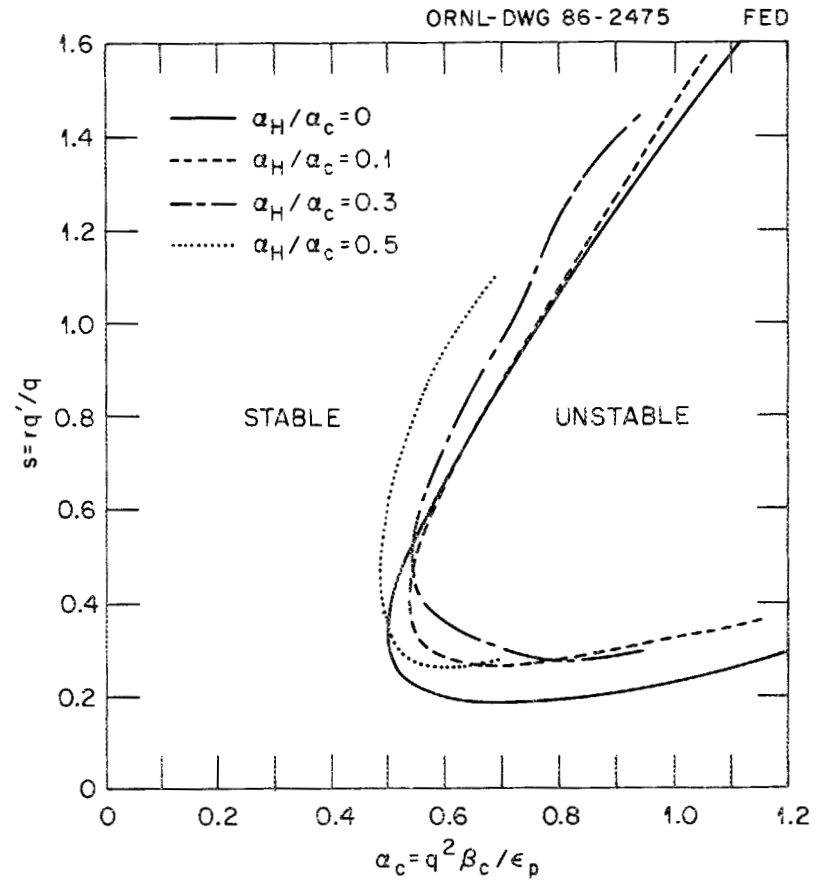


Fig. 4. Marginal stability boundaries for  $\alpha_H/\alpha_c = 0, 0.1, 0.3,$  and  $0.5$  for  $T_e = 20 \text{ keV}, \lambda_p/\alpha = 0.25, b_i = 0.04,$  and  $q = 1.7.$

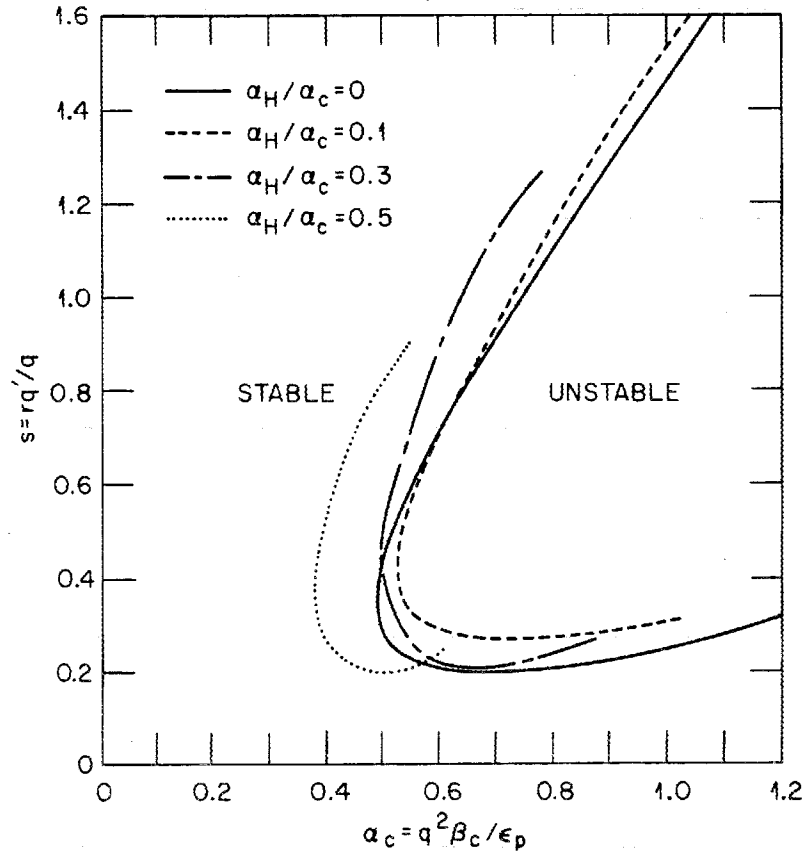


Fig. 5. Marginal stability boundaries for  $\alpha_H/\alpha_c = 0, 0.1, 0.3,$  and  $0.5$  for  $T_e = 30$  keV,  $\lambda_p/\alpha = 0.25,$   $b_i = 0.04,$  and  $q = 1.7.$

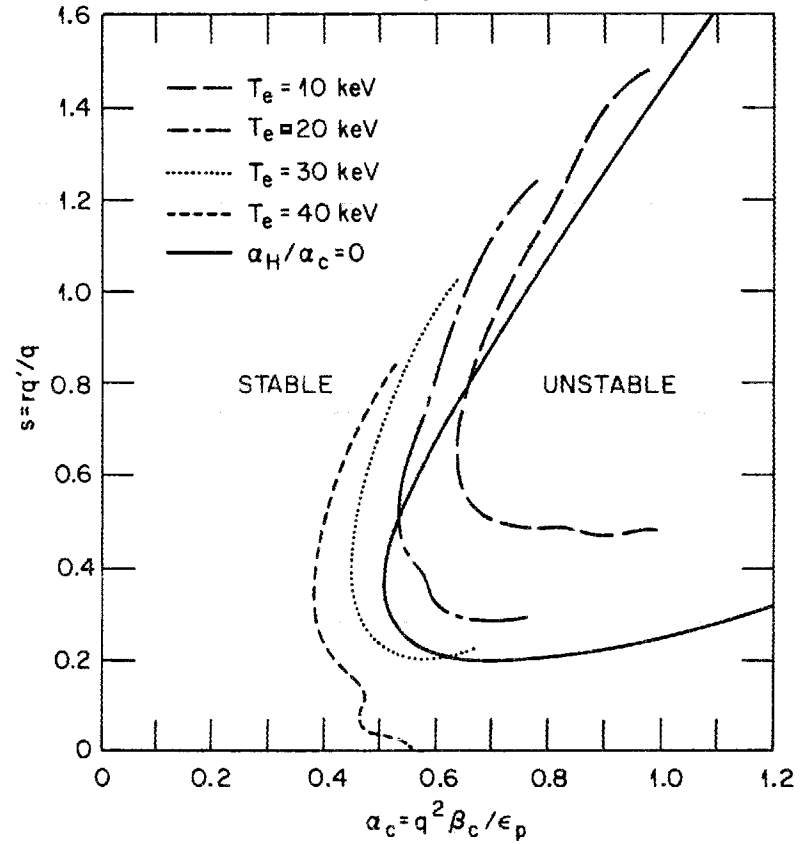


Fig. 6. Marginal stability boundaries for  $\alpha_H/\alpha_c = 0.3,$   $T_e = 10, 20, 30,$  and  $40$  keV,  $\lambda_p/\alpha = 0.25,$   $b_i = 0.04,$  and  $q = 1.7.$  Also, the case with no hot component is shown ( $\alpha_H/\alpha_c = 0,$  solid line).

iterative solution of the full coupled equations is then compared with this in Figs. 7 and 8 over a limited parameter range, indicating satisfactory agreement with respect to the dependence on shear. The iterative approach involves quite a bit more computer time to solve and has not at this time been used over as wide a parameter range. Having this more exact solution, however, has been useful in refining the accuracy of the approximate method.

In Fig. 3 we first examine dependence of marginal stability curves on the equilibrium parameter  $\lambda_p$ , which was defined following Eqs. (9)-(15). The value  $\lambda_p = 0.25\alpha$  (where  $\alpha = \alpha_c + \alpha_H$ ) is associated with a parabolic pressure profile, while  $\lambda_p = 0$  reduces to the equilibrium of Ref. [10]. Other parameters used here are  $\alpha_H/\alpha_c = 0.3$ ,  $T_e = 20$  keV,  $q = 1.7$ , and  $b_i = 0.04$ . As may be seen, increasing  $\lambda_p/\alpha$  monotonically stabilizes the first stability  $\beta$  limit. This effect is related to the increasing shift of the flux surface, modifying the curvature experienced by the plasma in the favorable direction. However, on the lower right-hand side of the unstable region, raising  $\lambda_p$  tends to destabilize the ballooning boundary;  $\lambda_p$  also can be thought of as a flux surface label, with the larger values representing flux surfaces closer to the edge. A typical trajectory through the  $s$ ,  $\alpha_c$ ,  $\lambda_p/\alpha$  parameter space would then start at  $\alpha_c = 0$ ,  $s = 0$ ,  $\lambda_p/\alpha = 0$  and move outward, increasing  $\alpha_c$ ,  $s$ , and  $\lambda_p/\alpha$  simultaneously up to some maximum  $\alpha_c$  (at the inflection point of the pressure profile) and then return back to the  $\alpha_c = 0$  axis, while continuing to increase  $s$  and  $\lambda_p/\alpha$ . A complete characterization of the stability of such an equilibrium would involve examining the unstable region in the three-dimensional  $s$ ,  $\alpha_c$ ,  $\lambda_p/\alpha$  parameter space. In the plots we

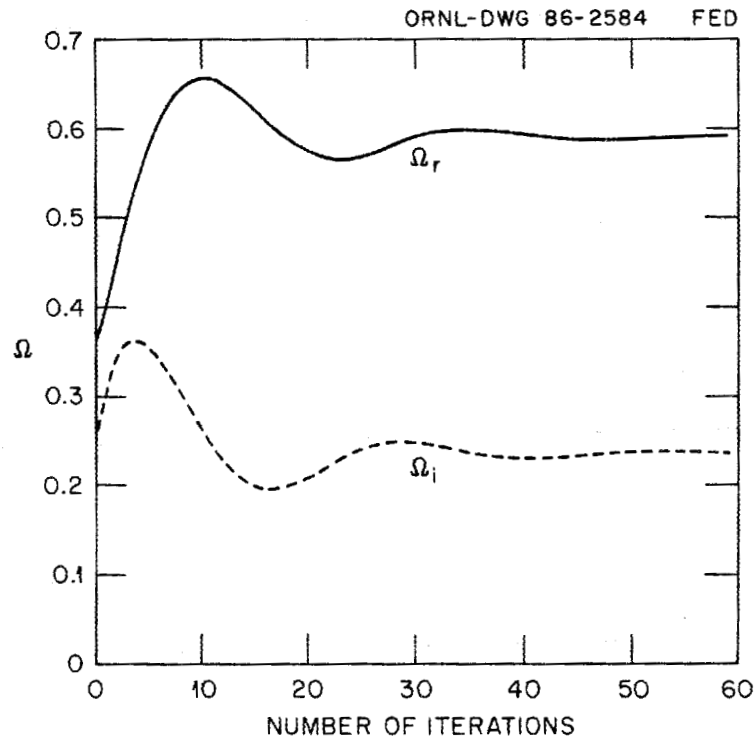


Fig. 7. Convergence study of iterative solution of Eqs. (16) and (17) for  $\alpha_H/\alpha_C = 0.3$ ,  $\alpha_C = 0.8$ ,  $s = 0.6$ ,  $T_e = 40$  keV,  $q = 2$ , and  $\lambda_p/\alpha = 0.25$ .

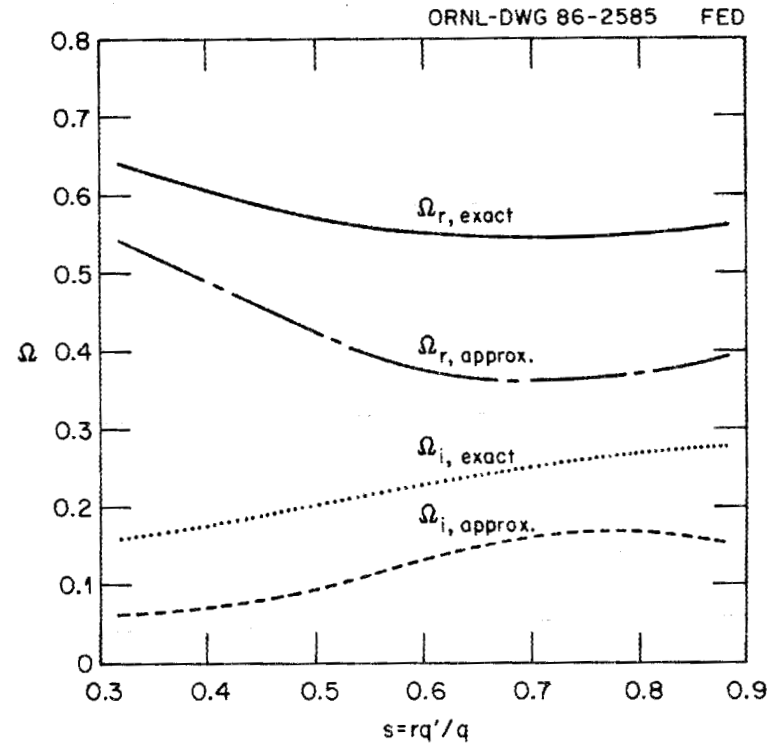


Fig. 8. Dependence of eigenvalues of approximate Eq. (26) and of full coupled Eqs. (16) and (17) on shear for  $\alpha_C = 0.8$ ,  $\alpha_H/\alpha_C = 0.3$ ,  $T_e = 40$  keV,  $q = 2$ , and  $\lambda_p/\alpha = 0.25$ .

generally fix  $\lambda_p/\alpha$  at 0.25 and study the dependences of stability boundaries on other parameters in  $s-\alpha_c$  space. However, in translating these results to a range of flux surfaces it would be necessary to map out the  $\lambda/\alpha$  dependence as is shown in Fig. 3 for a particular case.

In Figs. 4 and 5 the sensitivity of the stability boundaries to  $\alpha_H/\alpha_c$  is displayed for two values of background electron temperature,  $T_e = 20$  and 30 keV. At both values increasing the alpha pressure gradient relative to that of the background destabilizes the first stability boundary (left-hand region of the unstable region) and stabilizes the lower right-hand portion of the boundary. A somewhat greater effect is observed at 30 keV (Fig. 5) due to the stronger coupling between the background and hot species (i.e., the  $\omega \approx \langle\omega_{dH}\rangle$  resonance intercepts a greater fraction of the hot species distribution).

This feature is indicated more clearly in Fig. 6, where we have fixed the ratio  $\alpha_H/\alpha_c$  at 0.4 and varied  $T_e$ . Raising  $T_e$  increases the mean energy of the hot species distribution (due to increasing  $v_c/v_\alpha$ ). However, due to the choice of  $T_i = T_e$ , the location of the resonance between  $\langle\omega_{dH}\rangle$  and  $\omega_r$  (which is related to  $\omega_{*i}$  and thus  $T_i$ ) also moves to higher energies with increasing  $T_e$ . The net effect is to increase the strength of the coupling at  $\omega_r = \langle\omega_{dH}\rangle$  as a result of the increasing size of the  $H(\eta, \delta)$  function integrand with energy [i.e.,  $v^6/(v_c^3 + v^3)$ ]. As a result, increasing  $T_e$  lowers the first stability limit and also eventually closes access between first and second stable regions (e.g., notice the  $T_e = 40$  keV case).

As may be seen by comparing Figs. 4 through 6 with analogous ones from the deeply trapped limit [8], the isotropic distribution does not produce nearly as much destabilization. This may be attributed to the

more equal averaging over favorable and unfavorable curvature, which is present in the latter case. This feature primarily enters in through the right-hand side of Eq. (26), which is proportional to the bracket-bar average of the curvature-weighted potential  $\phi$ . It is also present in the pressure gradient-curvature drive term on the left-hand side of the mode equation. In the deeply trapped limit, the peaked anisotropic pressure distribution strongly weighted the unfavorable curvature near  $\theta = 2m\pi$ ,  $m = 0, 1, 2, \dots$ . For the isotropic model the hot pressure is constant along  $\theta$  and more evenly weights good and bad curvature regions.

We now turn to the iterative solution of the full set of Eqs. (16) and (17). In Fig. 7 a convergence study of  $\Omega_r$  and  $\Omega_i$  is shown based on the parameters  $s = 0.6$ ,  $\alpha_c = 0.8$ ,  $T_e = 40$  keV,  $q = 2$ ,  $\frac{\alpha_H}{\alpha_c} = 0.3$ , and  $\lambda_p = 0.25\alpha$ ;  $\phi$ ,  $Q_{||}$ , and the eigenvalues are initially determined using the approximate method based on Eq. (26). The code is then run for about 60 iterations, indicating a reasonably well converged solution at this point. Both the initial growth rate and real frequency are below the final values in this case, with  $\Omega_r$  changing more than  $\Omega_i$ . A similar characteristic is seen in Fig. 8 where the dependence of roots of the more exact Eqs. (16) and (17) is compared with that of Eq. (26) as a function of  $s$  at fixed  $\alpha_c = 0.8$ ,  $T_e = 40$  keV, and  $\alpha_H/\alpha_c = 0.3$ . However, the qualitative dependence on  $s$  is similar in the two calculations.

## 5. CONCLUSIONS

In this report we have developed the basic equations and numerical solution methods for examining the effects of an isotropic alpha distribution on tokamak ballooning modes. In addition, this approach can be extended to the case of anisotropic distributions. Applying these equations to parameters characteristic of break-even and ignition tokamaks generally indicates that energetic alpha populations can destabilize the first stability beta limit. This is similar to the destabilization observed in earlier calculations [1,8] based on a deeply trapped alpha model, but not nearly as strong. The greater destabilization of the latter model can be understood from its dominant weighting of the unfavorable curvature on the outside of the tokamak.

Our results indicate several ways to alleviate this destabilization and, in some cases, possibilities for improving stability over the case with no alphas present. First, as was shown in Fig. 3, operation with larger values of the  $\lambda_p$  parameter (proportional to the flux surface shift and to  $\epsilon\beta_p$ ) is stabilizing. Second, from Figs. 4 and 5, limiting the ratio of the alpha pressure gradient to the background pressure gradient weakens the effect of the alphas. Finally, keeping the background electron temperature  $T_e$  below some maximum value is desirable (Fig. 6). In fact, for  $T_e \leq 20$  keV, increased access between first and second stable regions is possible. The increasing destabilization with rising electron temperature shown in Fig. 6 may also be useful for burn control in a thermally unstable ignited plasma.

Comparison of the isotropic alpha pitch angle and deeply trapped alpha results indicates that the deeply trapped portion of the alpha

distribution plays an important role in the observed destabilization. In the tokamak this part of the alpha distribution could be depleted by adding a small amount of ripple in the toroidal field. Of course, there would be a trade-off between the adverse effects on the alpha energy balance and the possibility of improving the ballooning beta limit. The analysis and solution methods of this report could be applied to stability aspects of such a problem through consideration of an  $F_\lambda$  distribution which is hollowed out near  $\lambda = 1$ .

## REFERENCES

1. D. A. Spong, D. J. Sigmar, W. A. Cooper, and D. E. Hastings, *Phys. Fluids* 28, 2494 (1985).
2. J. Wieland and L. Chen, *Phys. Fluids* 28, 1359 (1985).
3. G. Rewoldt and W. M. Tang, *Nuclear Fusion* 24, 1573 (1984).
4. L. Chen, R. B. White, and M. N. Rosenbluth, *Phys. Rev. Lett.* 52, 1122 (1984).
5. K. McGuire, R. Goldston, M. Bell, M. Bitter, K. Bol, K. Brau, D. Buchenauer, T. Crowley, S. Davis, F. Dylla, H. Eubank, H. Fishman, R. Fonck, B. Grek, R. Grimm, R. Hawryluk, H. Hsuan, R. Hulse, R. Izzo, R. Kaita, S. Kaye, H. Kugel, D. Johnson, J. Manickam, D. Manos, D. Mansfield, E. Mazzucato, R. McCann, D. McCune, D. Monticello, R. Motley, D. Mueller, K. Oasa, M. Okabayashi, K. Owens, W. Park, M. Reusch, N. Sauthoff, G. Schmidt, S. Sesnic, J. Strachan, C. Surko, R. Slusher, H. Takahaski, F. Tenney, H. Towner, J. Valley, and R. White, *Phys. Rev. Lett.* 50, 891 (1983).
6. M. N. Rosenbluth, S. T. Tsai, J. W. Van Dam, and M. G. Engquist, *Phys. Rev. Lett.* 51, 1967 (1983).
7. J. W. Connor, R. J. Hastie, T. J. Martin, and M. F. Turner, *Proceedings of the Third Joint Varenna-Grenoble International Symposium on Heating in Toroidal Plasmas*, vol. 1, p. 65. *Comm. of the European Communities*, Brussels, 1982.
8. D. A. Spong, D. E. Hastings, D. J. Sigmar, and W. A. Cooper, see National Technical Information Service Document No. DE86004647 (Oak Ridge National Laboratory Report ORNL/TM-9688).

9. P. J. Catto, R. J. Hastie, and J. W. Connor, Plasma Phys. Controlled Fusion 27, 307 (1985).
10. J. W. Connor, R. J. Hastie, and J. B. Taylor, Phys. Rev. Lett. 40, 396 (1978).
11. B. Coppi, G. B. Crew, and J. J. Ramos, Comments Plasma Phys. Controlled Fusion 8, 11 (1983); also see B. Coppi, A. Ferreira, J. W.-K. Mark, and J. J. Ramos, Nucl. Fusion 19, 715 (1979).
12. S. P. Hirshman and J. C. Whitson, Phys. Fluids 26, 3553 (1983).



**INTERNAL DISTRIBUTION**

- |                    |   |
|--------------------|---|
| 1. D. B. Batchelor | 15. J. F. Lyon                                    |
| 2. C. O. Beasley   | 16. J. A. Rome                                    |
| 3. B. A. Carreras  | 17. K. C. Shaing                                  |
| 4. M. D. Carter    | 18. J. Sheffield                                  |
| 5. E. C. Crume     | 19-24. D. A. Spong                                |
| 6. N. O. Dominguez | 25-26. Laboratory Records Department              |
| 7. R. A. Dory      | 27. Laboratory Records, ORNL-RC                   |
| 8. C. L. Hedrick   | 28. ORNL Patent Office                            |
| 9. S. P. Hirshman  | 29. Document Reference Section                    |
| 10. J. T. Hogan    | 30. Central Research Library                      |
| 11. W. A. Houlberg | 31. Fusion Energy Division Library                |
| 12. H. C. Howe     | 32. Fusion Energy Division<br>Publications Office |
| 13. E. F. Jaeger   |   |
| 14. G. S. Lee      |   |

**EXTERNAL DISTRIBUTION**

33. Office of the Assistant Manager for Energy Research and Development, Department of Energy, Oak Ridge Operations Office, P.O. Box E, Oak Ridge, TN 37831
34. J. D. Callen, Department of Nuclear Engineering, University of Wisconsin, Madison, WI 53706
35. R. W. Conn, Department of Chemical, Nuclear, and Thermal Engineering, University of California, Los Angeles, CA 90024
36. S. O. Dean, Fusion Power Associates, 2 Professional Drive, Suite 248, Gaithersburg, MD 20879
37. H. K. Forsen, Bechtel Group, Inc., Research & Engineering, P.O. Box 3965, San Francisco, CA 94119
38. A. Fruchtman, Courant Institute of Mathematical Sciences, New York University, 251 Mercer Street, New York, NY 10012
39. R. W. Gould, Department of Applied Physics, California Institute of Technology, Pasadena, CA 91125
40. D. G. McAlees, Exxon Nuclear Co., Inc., 777 106th Avenue, NE, Bellevue, WA 98009
41. K. Riedel, Courant Institute of Mathematical Sciences, New York University, New York, NY 10012

42. H. Weitzner, Courant Institute of Mathematical Sciences, New York University, New York, NY 10012
43. P. J. Reardon, Princeton Plasma Physics Laboratory, P.O. Box 451, Princeton, NJ 08544
44. W. M. Stacey, School of Nuclear Engineering, Georgia Institute of Technology, Atlanta, GA 30332
45. G. A. Eliseev, I. V. Kurchatov Institute of Atomic Energy, P.O. Box 3402, 123182 Moscow, U.S.S.R.
46. V. A. Glukhikh, Scientific-Research Institute of Electro-Physical Apparatus, 188631 Leningrad, U.S.S.R.
47. I. Spighel, Lebedev Physical Institute, Leninsky Prospect 53, 117924 Moscow, U.S.S.R.
48. D. D. Ryutov, Institute of Nuclear Physics, Siberian Branch of the Academy of Sciences of the U.S.S.R., Sovetskaya St. 5, 630090 Novosibirsk, U.S.S.R.
49. V. T. Tolok, Kharkov Physico-Technical Institute, Academical St. 1, 310108 Kharkov, U.S.S.R.
50. R. Varma, Physical Research Laboratory, Navangpura, Ahmedabad, India
51. Bibliothek, Max-Planck Institut fur Plasmaphysik, D-8046 Garching bei Munchen, Federal Republic of Germany
52. Bibliothek, Institut fur Plasmaphysik, KFA, Postfach 1913, D-5170 Julich, Federal Republic of Germany
53. Bibliotheque, Centre de Recherches en Physique des Plasmas, 21 Avenue des Bains, 1007 Lausanne, Switzerland
54. Bibliotheque, Service du Confinement des Plasmas, CEA, B.P. No. 6, 92 Fontenay-aux-Roses (Seine), France
55. Documentation S.I.G.N., Departement de la Physique du Plasma et de la Fusion Controlee, Centre d'Etudes Nucleaires, B.P. 85, Centre du Tri, 38041 Cedex, Grenoble, France
56. Library, Culham Laboratory, UKAEA, Abingdon, Oxon, OX14 3DB, England
57. Library, FOM-Instituut voor Plasma-Fysica, Rijnhuizen, Jutphaas, The Netherlands
58. Library, Institute of Physics, Academia Sinica, Beijing, Peoples Republic of China
59. Library, Institute of Plasma Physics, Nagoya University, Nagoya, Japan
60. Library, International Centre for Theoretical Physics, Trieste, Italy
61. Library, Laboratorio Gas Ionizzati, Frascati, Italy
62. Library, Plasma Physics Laboratory, Kyoto University, Gokasho Uji, Kyoto, Japan
63. Plasma Research Laboratory, Australian National University, P.O. Box 4, Canberra, A.C.T. 2000, Australia

64. Thermonuclear Library, Japan Atomic Energy Research Institute, Tokai, Naka, Ibaraki, Japan
65. J. F. Clarke, Associate Director for Fusion Energy, Office of Fusion Energy, Office of Energy Research, U.S. Department of Energy, Mail Stop G-256, Washington, DC 20545
66. D. B. Nelson, Acting Director, Division of Applied Plasma Physics, Office of Fusion Energy, Office of Energy Research, U.S. Department of Energy, Mail Stop G-256, Washington, DC 20545
67. W. Sadowski, Fusion Theory and Computer Services Branch, Office of Fusion Energy, Office of Energy Research, U.S. Department of Energy, Mail Stop G-256, Washington, DC 20545
68. N. A. Davies, Tokamak Systems Branch, Office of Fusion Energy, Office of Energy Research, U.S. Department of Energy, Mail Stop G-256, Washington, DC 20545
69. E. Oktay, Tokamak Systems Branch, Office of Fusion Energy, Office of Energy Research, U.S. Department of Energy, Mail Stop G-256, Washington, DC 20545
70. M. N. Rosenbluth, University of Texas, Institute for Fusion Studies, RLM 11.218, Austin, TX 78712
71. Theory Department Read File, c/o D. W. Ross, University of Texas, Institute for Fusion Studies, Austin, TX 78712
72. Theory Department Read File, c/o R. C. Davidson, Director, Plasma Fusion Center, NW 16-202, Massachusetts Institute of Technology, Cambridge, MA 02139
73. Theory Department Read File, c/o F. W. Perkins, Princeton Plasma Physics Laboratory, P.O. Box 451, Princeton, NJ 08544
74. Theory Department Read File, c/o L. Kovrizhnikh, Lebedev Institute of Physics, Academy of Sciences, 53 Leninsky Prospect, 117924 Moscow, U.S.S.R.
75. Theory Department Read File, c/o B. B. Kadomtsev, I. V. Kurchatov Institute of Atomic Energy, P.O. Box 3402, 123182 Moscow, U.S.S.R.
76. Theory Department Read File, c/o T. Kamimura, Institute of Plasma Physics, Nagoya University, Nagoya, Japan
77. Theory Department Read File, c/o C. Mercier, Euratom-CEA, Service des Recherches sur la Fusion Controlée, Fontenay-aux-Roses (Seine), France
78. Theory Department Read File, c/o T. E. Stringer, JET Joint Undertaking, Culham Laboratory, Abingdon, Oxon OX14 3DB, England
79. Theory Department Read File, c/o K. Roberts, Culham Laboratory, Abingdon, Oxon OX14 3DB, England
80. Theory Department Read File, c/o D. Biskamp, Max Planck Institut für Plasmaphysik, D-8046 Garching bei München, Federal Republic of Germany

81. Theory Department Read File, c/o T. Takeda, Japan Atomic Energy Research Institute, Tokai, Naka, Ibaraki, Japan
82. Theory Department Read File, c/o C. S. Liu, GA Technologies, Inc., P.O. Box 81608, San Diego, CA 92138
83. Theory Department Read File, c/o L. D. Pearlstein, Lawrence Livermore National Laboratory, P.O. Box 808, Livermore, CA 94550
84. Theory Department Read File, c/o R. Gerwin, CTR Division, Los Alamos National Laboratory, P.O. Box 1663, Los Alamos, NM 87545
85. T. Amano, Institute of Plasma Physics, Nagoya University, Nagoya, Japan
86. C. D. Boley, Fusion Power Program, Building 207C, Argonne National Laboratory, Argonne, IL 60439
87. Yu. N. Dnestrovskii, I. V. Kurchatov Institute of Atomic Energy, P.O. Box 3402, 123182 Moscow, U.S.S.R.
88. J. Gaffey, IPST, University of Maryland, College Park, MD 20742
89. R. J. Hawryluk, Princeton Plasma Physics Laboratory, P.O. Box 451, Princeton, NJ 08544
90. W. W. Pfeiffer, GA Technologies, Inc., P.O. Box 81608, San Diego, CA 92138
91. D. E. Post, Princeton Plasma Physics Laboratory, P.O. Box 451, Princeton, NJ 08544
92. A. Ware, Physics Department, University of Texas, Austin, TX 78712
93. J. Wiley, University of Texas, Institute for Fusion Studies, Austin, TX 78712
94. S. K. Wong, GA Technologies, Inc., P.O. Box 81608, San Diego, CA 92138
95. S. Yoshikawa, Princeton Plasma Physics Laboratory, P.O. Box 451, Princeton, NJ 08544
96. Duk-In Choi, Department of Physics, Korea Advanced Institute of Science and Technology, P.O. Box 150, Chong Ryang-Ri, Seoul, Korea
97. J. W. Van Dam, Institute for Fusion Studies, University of Texas, Austin, TX 78712
98. H. L. Berk, Institute for Fusion Studies, University of Texas, Austin, TX 78712
99. O. J. Kwon, Institute for Fusion Studies, University of Texas, Austin, TX 78712
100. R. Carrera, Institute for Fusion Studies, University of Texas, Austin, TX 78712
101. X. Llobet, Institute for Fusion Studies, University of Texas, Austin, TX 78712
102. A. Punjabi, Mathematics Department, Hampton University, Hampton, VA 23668
103. G. Burkhart, LPF, University of Maryland, College Park, MD 20742

104. C. Z. Cheng, Princeton University, PPPL, P.O. Box 451, Princeton, NJ 08544
105. H. Biglari, Princeton University, PPPL, P.O. Box 451, Princeton, NJ 08544
106. D. P. Stotler, Princeton University, PPPL, P.O. Box 451, Princeton, NJ 08544
107. D. E. Hastings, Plasma Fusion Center, Massachusetts Institute of Technology, NW16-243, 167 Albany St., Cambridge, MA 02139
108. J. J. Ramos, Plasma Fusion Center, Massachusetts Institute of Technology, NW16-243, 167 Albany St., Cambridge, MA 02139
- 109-113. D. J. Sigmar, Plasma Fusion Center, Massachusetts Institute of Technology, NW16-243, 167 Albany St., Cambridge, MA 02139
114. K. T. Tsang, SAIC, P.O. Box 2351, La Jolla, CA 92038
115. W. A. Cooper, Centre de Recherches en Physique des Plasmas, CH-1007, Lausanne, Switzerland
- 116-249. Given distribution as shown in TIC-4500, Magnetic Fusion Energy (Distribution Category UC-20g, Theoretical Plasma Physics)